ACS APPLIED ENERGY MATERIALS

www.acsaem.org Letter

# Flash Lamp Annealing Enables Thin-Film Solid-State Batteries on Aluminum Foil

Xubin Chen,[‡] Jordi Sastre,[*,‡] Abdessalem Aribia, Evgeniia Gilshtein, and Yaroslav E. Romanyuk[*]

Cite This: *ACS Appl. Energy Mater.* 2021, 4, 5408−5414 Read Online

ACCESS | Metrics & More | Article Recommendations

**ABSTRACT:** Crystallization of cathode films in solid-state microbatteries requires thermal annealing at high temperatures, restricting the choice of substrate and current collector materials. Here, flash lamp annealing (FLA) is explored to crystallize $LiCoO_2$ (LCO) cathodes on aluminum foils. Millisecond pulses of visible light induce rapid heating of the LCO films up to 900 °C, whereas the aluminum never exceeds the melting point. Microbatteries consisting of an FLA-processed LCO cathode, a LiPON electrolyte, and a Li metal anode are fabricated on flexible aluminum foil, with performance comparable to those on rigid silicon. This method can enable new microbattery designs at lower production costs.

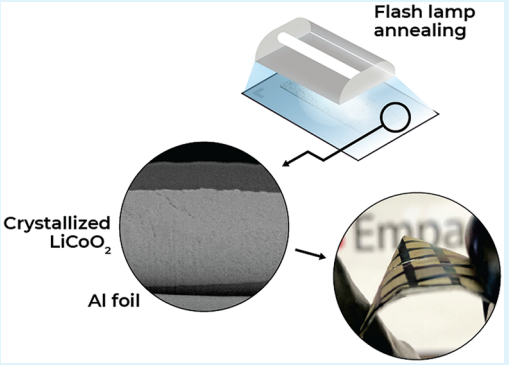


**KEYWORDS:** *thin-film solid-state batteries, microbatteries, flexible batteries, flash lamp annealing, lithium cobalt oxide*



Thin-film solid-state batteries (TF-SSBs) are marketed as an integrated energy storage unit for low-power devices such as wearable sensors, smart cards, implantable medical devices, and active radio frequency identification (RFID) tags.[1] They provide energy and power densities in the range of mWh and mW, respectively, ideal for electronic systems where the power consumption is in the $\mu$W range (e.g., 3 $\mu$W for a glucose sensor).[2−5] The development and expansion of the Internet of Things (IoT), wearables, and ubiquitous sensing will require better and cheaper TF-SSBs. Indeed, the market of flexible, printed, and thin-film batteries is expected to reach a size of $500 million by 2030.[6] In the fabrication of TF-SSBs, the cell components are sequentially deposited in the form of films onto a substrate. To obtain an electrochemically active cathode with high capacity, the film made of a cathode material, such as the spinel $LiMn_2O_4$ (LMO),[7] layered $LiCoO_2$ (LCO),[8] or olivine $LiFePO_4$ (LFP), needs to be crystallized after deposition. This crystallization step is typically done by annealing the cathode/current collector/substrate stack in a furnace at temperatures about 700 °C for several hours.[9] Such thermal annealing adds cost and complexity to the fabrication process and, importantly, limits the substrate choice to temperature-resistive materials like Si, sapphire, or special stainless steels.

If a temperature-sensitive substrate (e.g., Al foil or a polymer) is used for the fabrication of TF-SSBs, either an amorphous cathode material with a lower potential (e.g., $MoO_3$ with ∼1.7 V vs $Li^+/Li$)[10,11] has to be used or the annealing temperature needs to be decreased to a suboptimal value. In both cases, the ion kinetics in the cathode becomes slower, and therefore the thickness of the cathode film has to be limited to submicrometer values, which restricts the areal capacity of the batteries to below 100 $\mu$W h $cm^{-2}$. TF-SSBs on flexible ceramic substrates such as Y−$ZrO_2$[12] and mica[13] have been demonstrated. These inorganic substrates can endure high temperatures (above 1000 °C) so that cathodes deposited on them can be fully crystallized. TF-SSBs with such substrate are able to deliver performances comparable to those on a rigid substrate. However, these ceramics have to be processed to thicknesses of about 100 $\mu$m to become flexible, adding high complexity to the processing, and even then, the flexibility is limited as compared to polymers and metallic foils. Additionally, a current collector layer has to be added between the ceramic and the cathode for electrical conduction. Common current collector materials for TF-SSBs are Pt and Au, which are unreactive and thermally stable at high processing temperatures as well as electrochemically stable during operation. An additional layer such as Cr and Ti is often needed between the ceramic and the current collector to improve adhesion.

**Received:** May 5, 2021
**Accepted:** June 7, 2021
**Published:** June 17, 2021

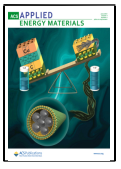





https://doi.org/10.1021/acsaem.1c01283
*ACS Appl. Energy Mater.* 2021, 4, 5408−5414

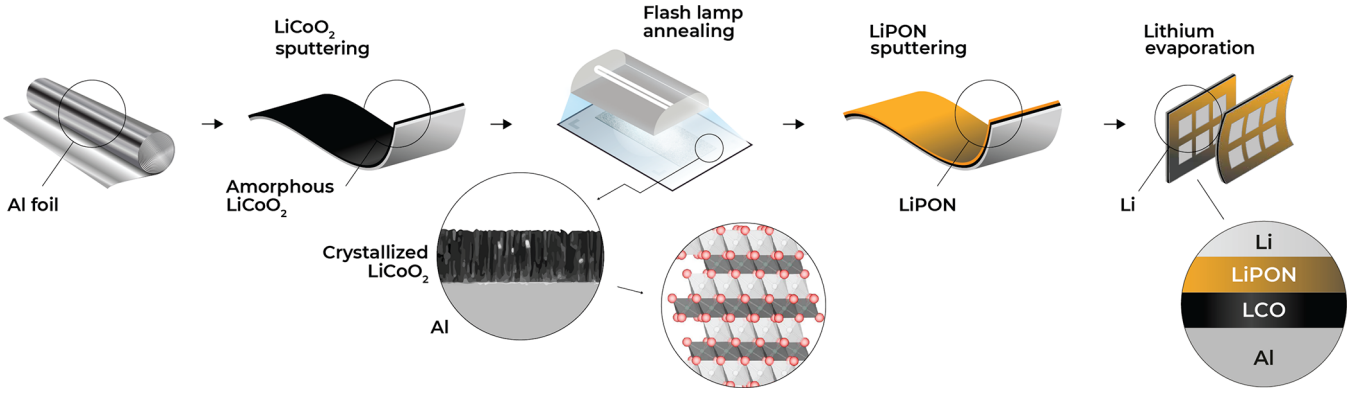


**Figure 1.** Processing steps for fabrication of TF-SSBs on Al foil.

Metallic substrates offer lower material cost, present flexibility, and do not require an additional current collector layer unlike polymer and ceramic substrates. Conventional Li-ion batteries employ Cu and Al as substrates for anode and cathode, respectively. Surface-passivated Al foil is electrochemically stable against high voltage cathodes and cost-effective from an industrial perspective. However, the use of Al foil as a substrate for TF-SSBs is impeded by its melting point of 660 °C and the cross-diffusion of Al and cathode components that degrade the electrode performance.

Novel photonic methods for cathode crystallization have been reported as a way to circumvent the temperature limitation. Our group recently published a comparison of three different methods (flash lamp, UV excimer laser, and IR laser annealing) for rapid crystallization of 150 nm LMO cathode films.[14] Yim et al.[15] utilized a UV excimer laser to crystallize 220 nm $LiNi_{0.5}Mn_{1.5}O_4$ (LNMO) cathode films on polyimide, but the TF-SSB could deliver only ∼20% of the theoretical capacity at a discharge rate of 0.4 C (corresponding to 70 $\mu$W h cm$^{-2}$ at 35 $\mu$W cm$^{-2}$).

In this study, we investigate the use of flash lamp annealing (FLA)[16] as a crystallization technique for fabrication of high-performance TF-SSBs on Al foil. FLA, also known as intense pulsed light (IPL) or photonic curing (PC), uses light pulses with a duration of 0.1−10 ms from a xenon pulsed lamp, which generates light with a broad spectral band ranging from the UV to the IR (200 nm to 1.5 $\mu$m in this work) for a rapid, transient heating of the illuminated surfaces. In FLA, only the upper layers of the sample are heated while the substrate is kept relatively cool, below the melting point, which is not possible in the traditional thermal annealing methods.

Figure 1 illustrates the fabrication steps to manufacture TF-SSBs on Al foil. LCO films with thicknesses of 0.7, 1.2, and 3.3 $\mu$m were sputtered directly on Al foil and subsequently crystallized by FLA. Neither additional adhesion layer nor interdiffusion barrier was required between the LCO film and the Al foil, which simplifies the fabrication process compared to those with polymer and ceramic substrates. Lithium phosphorus oxynitride (LiPON) and Li were used as electrolyte and anode, respectively, with an active device area of 3 × 5 mm$^2$.

The essential crystallization step of the LCO film was performed by FLA through consequent light pulses, using 20 pulses for 0.7 $\mu$m LCO, with a total output exposure energy density of 330 J cm$^{-2}$, 43 pulses for 1.2 $\mu$m LCO with 830 J cm$^{-2}$, and 300 pulses for 3.3 $\mu$m LCO with 4950 J cm$^{-2}$. These parameters were optimized for attaining a desired crystalline phase and electrochemical performance while avoiding damage to the Al foil. To estimate the temperatures reached on the surface of the LCO layer, the SimPulse software was used. The simulation results are shown in Figure 2. On the surface of the cathode, annealing temperatures ranging from 700 to 900 °C were estimated. Thicker films demand a higher surface temperature to ensure sufficient crystallization for good electrochemical performance of the cathode. Simultaneously, the Al substrate remained below the melting point of the Al foil (660 °C) for most of the experiments. This simulation confirms that the LCO films can be annealed without thermally loading the underlying Al substrate, which is the main advantage of the FLA method used in this study.

Figure 3a shows an optical picture of the bendable TF-SSBs on Al foil. After the FLA processing, the LCO films exhibit homogeneous microstructure, as seen in the secondary electron microscopy (SEM) image of the TF-SSB in Figure 3b. The surface of the FLA processed LCO remains smooth after FLA processing, and crystal grain-like features appear, evidencing crystallization of the cathode film. LCO adheres well to the Al foil, and no delamination is observed. The well-defined boundary between LCO and Al indicates negligible interdiffusion or cross reactions. The crystallization of LCO films with thickness ranging from 0.7 to 3.3 $\mu$m was verified by grazing-incidence X-ray diffraction (GI-XRD), comparing an as-sputtered LCO film with the FLA-processed films (Figure 3c). The as-sputtered film shows only reflexes of the Al substrate and a broad hump which can be attributed to the amorphous LCO phase. The reflections that appear in the FLA-processed LCO films can be indexed to a layered LCO phase, the desired electrochemically active phase. No secondary phases can be detected in the XRD patterns. The remaining hump at lower diffraction angles indicates that some amorphous phase is still present in the cathode film, likely at the lower part of the film due to the temperature gradient. The hump becomes larger for the thicker film, which is consistent with the assumption that a higher crystallinity is achieved in the surface layers. The higher background noise and broader peaks at low angles in the diffractogram of the 3.3 $\mu$m LCO film can also be caused by an increase of the surface roughness observed in the samples with thicker LCO films. To further investigate the interface between LCO and the Al foil, an elemental profile of the Al/1.2 $\mu$m LCO stack after FLA was acquired by time-of-flight secondary ion mass spectrometry (ToF-SIMS), as shown in Figure 3d. The signals corresponding to $^6Li^+$, $Co^+$, $Al^+$, and $Al^-$ rapidly decay when transitioning from one layer to the other, indicating low concentrations of Al


https://doi.org/10.1021/acsaem.1c01283
ACS Appl. Energy Mater. 2021, 4, 5408−5414

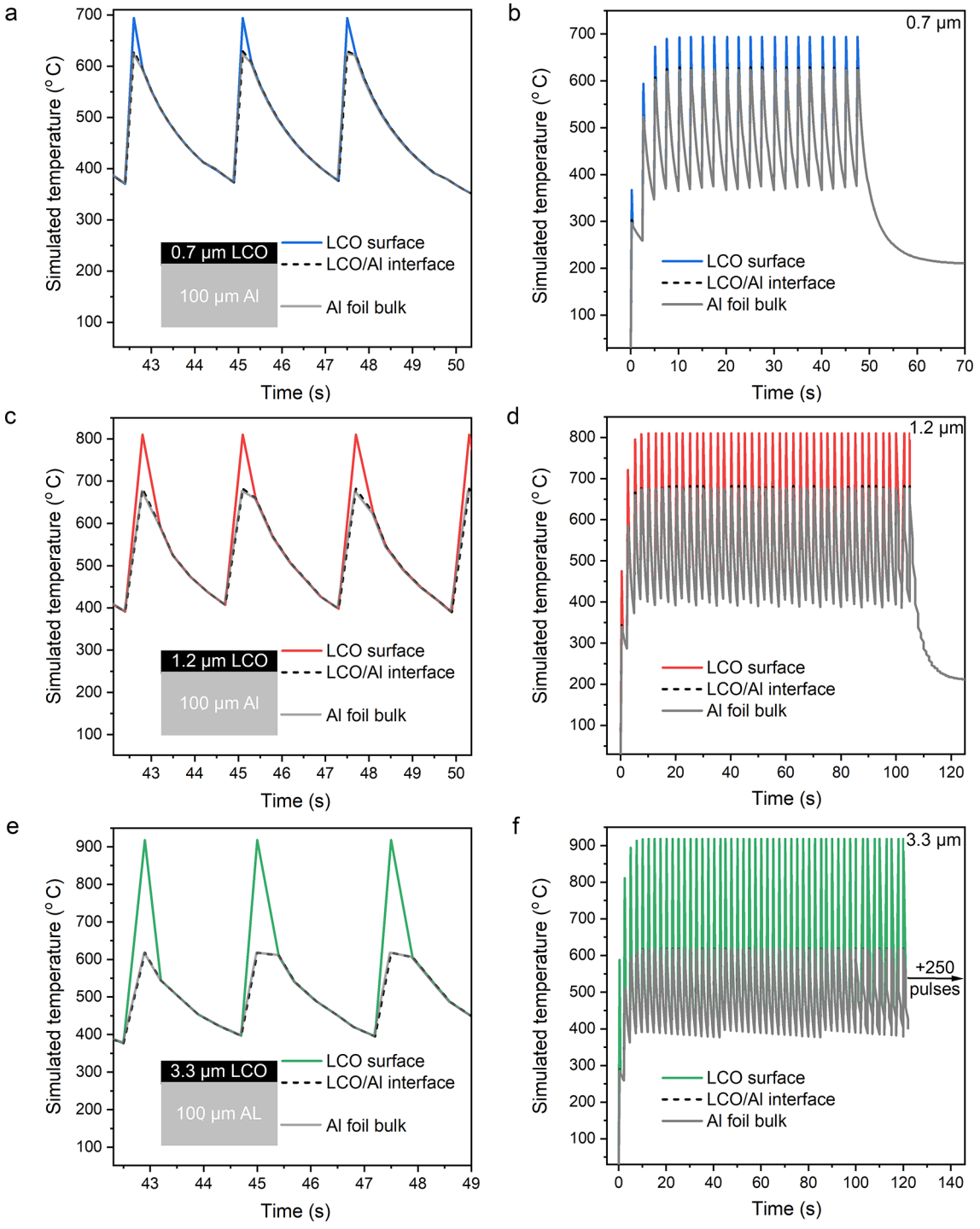


**Figure 2.** Simulated temperature profiles of FLA microsecond processing for (a,b) 0.7, (c,d) 1.2, and (e,f) 3.3 $\mu$m LCO films on Al foil, representing temperatures reached on the LCO surface, at the LCO/Al interface, and in the bulk of the Al foil. Left plots show three enlarged pulses after 42 s processing, and right plots show the complete temperature profile during the processing.

in the LCO layer and Co and Li in the Al foil. This evidence that no major elemental interdiffusion occurs during the FLA treatment.

The cyclovoltammetry measurement of a FLA-processed LCO film seen in Figure 4a shows peaks at around 3.9 V, which correspond to the characteristic lithiation and delithiation processes of crystalline LCO. The galvanostatic charge−discharge curves in Figure 4b also present the distinct lithiation and delithiation plateaus at about 3.9 V. The voltage profiles are similar for the three different thicknesses investigated, with an areal capacity scaling as a function of thickness. When charged/discharged at a rate of C/8, corresponding to a current density of 32 $\mu$A cm$^{-2}$, the 3.3 $\mu$m LCO electrode (3.3-LCO) is capable of delivering a capacity of 212 $\mu$A h cm$^{-2}$, corresponding to approximately 90% of the theoretical value. Normalized to the cathode thickness, this corresponds to a value of 64 $\mu$A h cm$^{-2}$ $\mu$m$^{-1}$. At about 1 C, corresponding respectively to 50 and 86 $\mu$A cm$^{-2}$ for the electrodes with a thickness of 0.7 $\mu$m (0.7-LCO) and 1.2 $\mu$m (1.2-LCO), the TF-SSBs deliver almost full


https://doi.org/10.1021/acsaem.1c01283
ACS Appl. Energy Mater. 2021, 4, 5408−5414

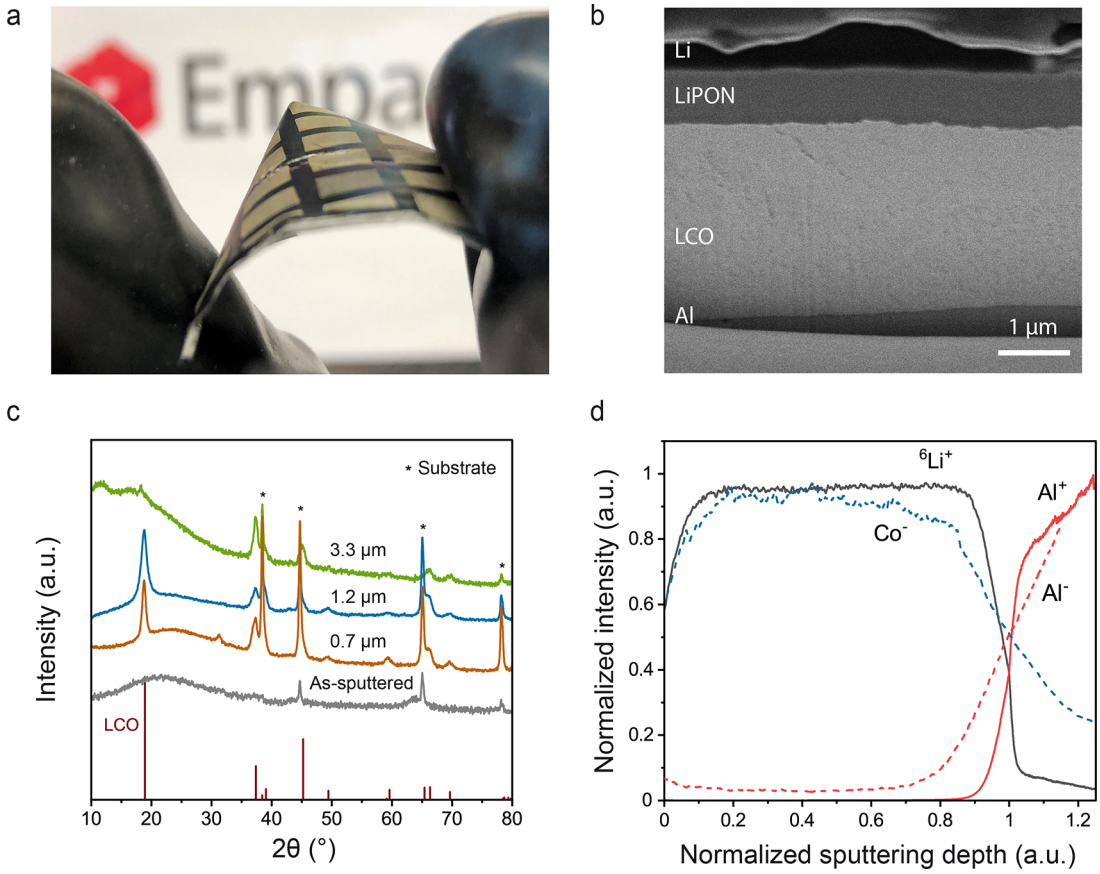


**Figure 3.** (a) Picture of an array of TF-SSBs on a bendable Al foil. (b) Cross-sectional SEM image of the TF-SSB with FLA-processed LCO. (c) GI-XRD diffractograms of an as-sputtered LCO film and FLA-crystallized LCO films with different thicknesses (0.7, 1.2, and 3.3 $\mu$m). (d) ToF-SIMS depth profile of an Al/1.2 $\mu$m LCO stack after FLA.

theoretical capacity of 49 and 85 $\mu$A h cm$^{-2}$, respectively. That is, 70 and 72 $\mu$A h cm$^{-2}$ $\mu$m$^{-1}$ when normalized to the cathode thickness. In contrast, the 3.3-LCO device loses about half the capacity at this rate as a result of the thicker cathode and a higher polarization. At about 10 °C, the capacity of the 0.7-LCO TF-SSB remains high at 30 $\mu$A h cm$^{-2}$, thanks to the shorter diffusion length through the thinner cathode film. At this same rate, the 1.2-LCO and 3.3-LCO TF-SSBs suffer a drop in capacity to 44 $\mu$A h cm$^{-2}$ and 46 $\mu$A h cm$^{-2}$, respectively, evidencing a downward trend in rate performance with the thickness of the electrode as a result of longer charge carrier diffusion paths. Regarding the cycle life, as shown in Figure 4c, the 1.7-LCO TF-SSBs exhibits almost no capacity fading after 100 cycles at 10 C.

Figure 4d shows a Ragone plot comparing the energy and power densities of the TF-SSBs fabricated in this work on Al foil (blue symbols), conventional TF-SSBs on rigid substrates (black symbols) and TF-SSBs fabricated on polymer and flexible ceramic substrates (brown symbols). Table 1 shows a detailed description of the architecture, processing conditions, and performance of selected TF-SSBs. All of the TF-SSBs presented in this plot employ LiPON as the electrolyte and lithium metal as the anode. The large disparity in performance between TF-SSBs fabricated on rigid sapphire or silicon substrates with Pt as current collector and TF-SSBs on flexible substrates becomes evident. The performance of the TF-SSBs on a flexible substrate is severely compromised by a lower thickness of the electrode and/or the use of amorphous cathodes. The only flexible TF-SSB with comparable performance to conventional TF-SSBs is the one fabricated on a thinned-down mica substrate. Thanks to the crystallized cathode obtained with the FLA processing, the TF-SSBs on bendable Al foil in this work show energy densities about 1 order of magnitude above those fabricated on polymers and, most remarkably, in the same range of those on costly sapphire/Pt substrates.

The TF-SSB with the thickest electrode can deliver an areal energy density of 828 $\mu$W h cm$^{-2}$ at a power of 123 $\mu$W cm$^{-2}$ and retains 22% of the areal energy density at powers as high as 5727 $\mu$W cm$^{-2}$. In contrast, the best reported TF-SSBs on polymer substrates discharged at such power densities fail to deliver energy densities above 15 $\mu$W h cm$^{-2}$.

The reported performance is sufficient to power microelectronic devices such as sensors that require energies and powers in the order of $\mu$W h and $\mu$W, respectively. To demonstrate the functionality of our batteries, a demonstrator with a 2 mA-rated light-emitting diode (LED) was built. As shown in Figure 4d, the green LED can be powered by a TF-SSB with a footprint of 0.15 cm$^2$.

In summary, we demonstrate a fabrication process of thin-film solid-state batteries with an LCO/LiPON/Li architecture on aluminum foil. The critical fabrication step is the flash lamp annealing of the LCO cathode films, enabling rapid surface heating under pulsed visible light. LCO films with a thickness up to 3.3 $\mu$m can be crystallized while the aluminum foil remains below the melting point, and no interdiffusion between LCO and Al takes place. The performance of the TF-SSBs on aluminum foil greatly exceeds previously reported


https://doi.org/10.1021/acsaem.1c01283
ACS Appl. Energy Mater. 2021, 4, 5408−5414

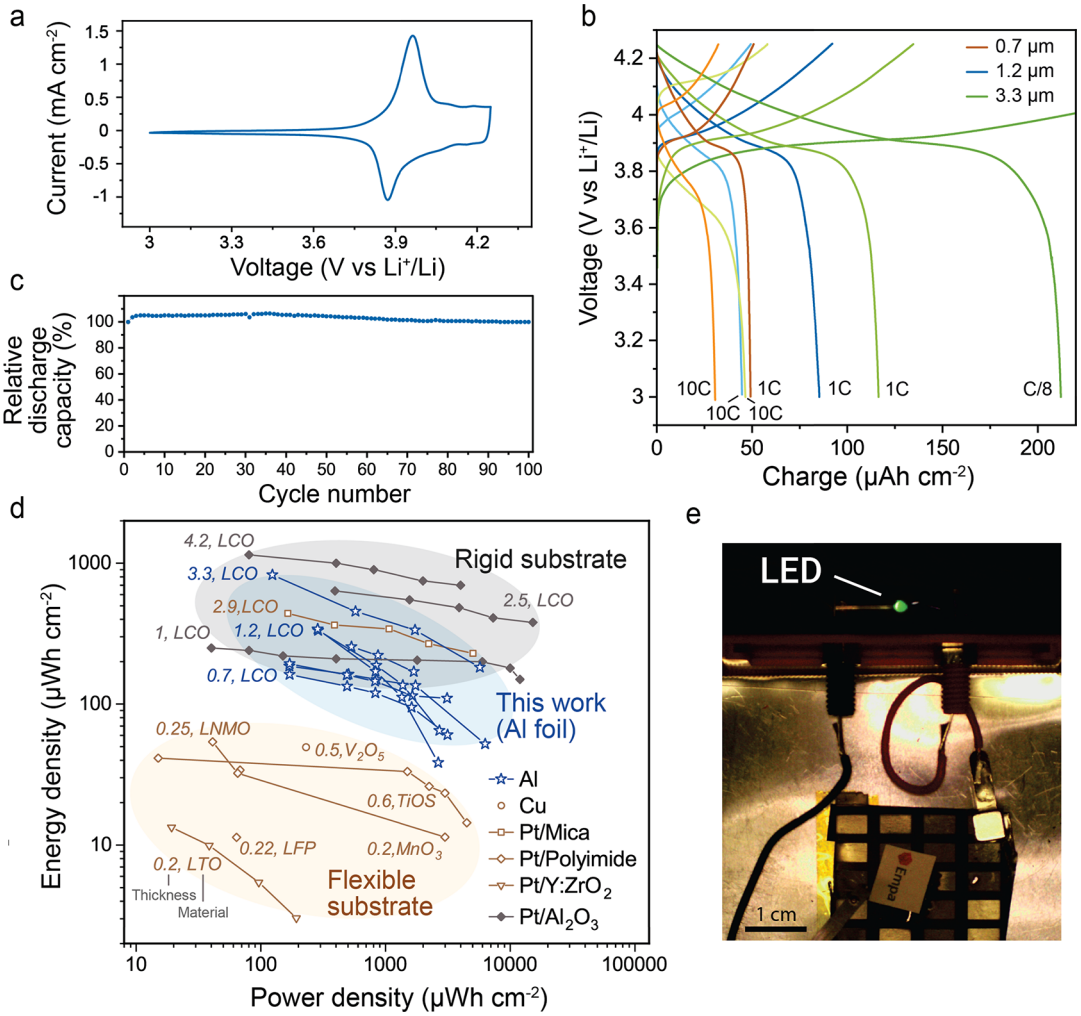


**Figure 4.** (a) Cyclovoltammetry measurement of a FLA-processed LCO film. (b) Charge−discharge curves at different C-rates of TF-SSBs with FLA-processed LCO films of different thicknesses. (c) Normalized discharge capacity over 100 cycles. (d) Ragone plot comparing the TF-SSBs on Al foil investigated in this work to state-of-the-art TF-SSBs on flexible and rigid substrates. (e) Picture of an LED powered by a TF-SSB on Al foil.

values for any flexible substrates. It is comparable to the state-of-the-art devices fabricated on sapphire or silicon wafers with a Pt current collector. Considering that the optical absorption and the crystallization profile of LCO are similar to those for other common cathode materials such as LFP, LNMO, and NMC, the described approach could be extended to these cathode materials as well. This approach presents an opportunity to realize new thin-film battery designs, which could be manufactured at a lower cost.

## METHODS

**TF-SSB Fabrication.** Aluminum foil (99.0%) with thickness of 0.1 mm (Korff AG) was used as substrate. As a cathode, $LiCoO_2$ films were deposited at room temperature by RF magnetron sputtering from a stoichiometric $LiCoO_2$ target (Toshima Manufacturing Co.) in an Orion sputtering system (AJA International Inc.) at a pressure of 3 Pa with a 24 sccm Ar + 1 sccm $O_2$ gas flow. The target was sputtered with a power of 5.9 W $cm^{-2}$. FLA was carried out using a PulseForge 1300 photonic curing system (Novacentrix). The pulse duration and frequency was set at 1.8 ms and 0.4 Hz, respectively. The 0.7 $\mu$m LCO film (0.7-LCO) was annealed with a bank voltage of 850 V and 20 light pulses, the 1.2 $\mu$m film (LCO-1.2) was annealed with a bank voltage of 900 V and 43 light pulses, and the 3.3 $\mu$m film (LCO-3.3) was annealed with a bank voltage of 850 V and 300 light pulses. As a solid electrolyte, LiPON films with a thickness of 1 $\mu$m were deposited at room temperature by RF magnetron sputtering by cosputtering a $Li_3PO_4$ target (Kurt J Lesker Co.) and a $Li_2O$ target (Toshima Manufacturing Co.) in an Orion sputtering system (AJA International Inc.) at a pressure of 0.4 Pa with a 50 sccm $N_2$ gas flow. The targets were sputtered with a power of 5 W $cm^{-2}$. The cosputtering of $Li_2O$ increases the lithiation of the LiPON film and improves its ionic conductivity. The ionic conductivity of the LiPON electrolyte is $2 \times 10^{-6}$ S $cm^{-1}$, as determined by EIS measurements with blocking electrodes. As the anode, 2 $\mu$m-thick Li films were thermally evaporated using a Nexdep evaporator (Angstrom Engineering Inc.). The Li films were deposited through shadow masks. Two device areas were used in this work: circles with a diameter of 0.1 cm (area of 0.008 $cm^2$) and rectangles with lateral dimensions of 0.3 cm by 0.5 cm (area of 0.15 $cm^2$).

**Simulation.** To estimate the temperatures reached on the surface of the LCO layer, the SimPulse software was used. It couples a transient 1-D heat conduction model to temperature-dependent thermal and optical material properties. For the simulations, the FLA pulses were treated as a volumetric source heat flux for the materials stack as shown in Figure 2: 100 $\mu$m thick Al foil with 0.7 $\mu$m, 1.2 $\mu$m, and 3.3 $\mu$m LCO layers. Thermal conductivity of 0.66 W $m^{-1}K^{-1}$, specific heat of 740 J $kg^{-1}$ $K^{-1}$, melting temperature of 1100 °C were used as input parameters for the LCO layer in the simulations.[22] Thermal conductivity of 237 W $m^{-1}$ $K^{-1}$, specific heat of 904 J $kg^{-1}$ $K^{-1}$, and melting temperature of 660 °C were used as input parameters for the aluminum substrate in the simulations.



https://doi.org/10.1021/acsaem.1c01283
ACS Appl. Energy Mater. 2021, 4, 5408−5414

**Table 1. Summary of State-of-the-Art TF-SSBs Fabricated on Non-noble Metal Current Collectors on Rigid Substrates or Flexible Current Collector/Substrates**

| | substrate/CC/cathode | electrolyte/anode | cathode fabrication | performance | ref |
|---|---|---|---|---|---|
| non-noble metallic current collector | Si/$Li_2O$, 20 nm Al/300−400 nm $LiCoO_2$ | wet half-cell measurement | sputtered, annealing at 500 °C, 2 h | 3.9 V, 40 $\mu$Ah $cm^{-2}$ $\mu m^{-1}$ @20 $\mu Acm^{-2}$ (1 C) | 17 |
| | 1.1 mm glass/100 nm V/200 nm $Li_2Mn_2O_4$ | 1.5 $\mu$m LiPON/ 50−300 nm $Nb_2O_5$ | sputtered, no annealing | 1.5 V, 60 $\mu$Ah $cm^{-2}$ $\mu m^{-1}$ @2 $\mu Acm^{-2}$ (~0.15 C), 500 cycles | 18 |
| flexible current collector/substrate | 160 $\mu$m glassor 75 $\mu$m polyimide/ 200 nm Pt/200 nm $MoO_3$ | 1.5 $\mu$m LiPON/7 $\mu$m Li | sputtered, no annealing | 1.7 V, 125 $\mu$Ah $cm^{-2}$ $\mu m^{-1}$ @10.1 $\mu Acm^{-2}$ (0.5 C) | 10,11 |
| | 30 $\mu$m SS (SUS304)/1.1 $\mu$m $LiCoO_2$ | wet half-cell measurement | sputtered, annealing at 550 °C, 20 min | 3.9 V, 37.56 $\mu$Ah $cm^{-2}$ $\mu m^{-1}$ @16 $\mu Acm^{-2}$ (~0.2 C), ~50 cycles | 19 |
| | 50 $\mu$m mica/Cr+Pt/3 $\mu$m $LiCoO_2$ | 1.5 $\mu$m LiPON/Li | sputtered, rapid annealing at 520 °C, 15 min | 3.9 V, 39 $\mu$Ah $cm^{-2}$ $\mu m^{-1}$ @42 $\mu Acm^{-2}$ (0.3 C), 800 cycles | 13 |
| | polyimide/250 nm Ti/600 nm TiOS | 1.4 $\mu$m LiPON/2 $\mu$m Li | sputtered, no annealing | 1.8 V, 78 $\mu$Ah $cm^{-2}$ $\mu m^{-1}$ @10 $\mu Acm^{-2}$ (0.2 C), >200 cycles | 20 |
| | polyimide/25 nm Ti + 80 nm Pt/ 250 nm LFP | 1.2 $\mu$m LiPON/2 $\mu$m Li | sputtered, annealing at 400 °C, 3 h | 3.4 V, 40 $\mu$Ah $cm^{-2}$ $\mu m^{-1}$ @10 $\mu Acm^{-2}$ (0.1 C), >70 cycles | 3,21 |
| | Polyimide/$SiO_2$−$Si_3N_4$, 50 nm Pt/ 220 nm LNMO | LiPON/Li | sputtered, UV excimer (70 mJ $cm^{-2}$) | 4.5 V, 12 $\mu$Ah $cm^{-2}$ $\mu m^{-1}$ @3.7 $\mu Acm^{-2}$ (0.4 C), >20 cycles | 15 |
| | 40 $\mu$m Y-$ZrO_2$/20 nm Ti + 70 nm Pt/200 nm LTO | 500 nm LiPON/Li | sputtered, annealing at 800 °C, 20 min | 1.6 V, 50 $\mu$Ah $cm^{-2}$ $\mu m^{-1}$ @120 $\mu Acm^{-2}$ (10 C) | 12 |
| | 100 $\mu$m Al foil/0.7 $\mu$m $LiCoO_2$ | 1 $\mu$m LiPON/2 $\mu$m Li | sputtered, FLA (330 J $cm^{-2}$) | 3.9 V, 70 $\mu$Ah $cm^{-2}$ $\mu m^{-1}$ @50 $\mu Acm^{-2}$ (1 C), >100 cycles | this work |
| | 100 $\mu$m Al foil/1.2 $\mu$m $LiCoO_2$ | 1 $\mu$m LiPON/2 $\mu$m Li | sputtered, FLA (830 J $cm^{-2}$) | 3.9 V, 72 $\mu$Ah $cm^{-2}$ $\mu m^{-1}$ @86 $\mu Acm^{-2}$ (1 C), >100 cycles | this work |
| | 100 $\mu$m Al foil/3.3 $\mu$m $LiCoO_2$ | 1 $\mu$m LiPON/2 $\mu$m Li | sputtered, FLA (4950 J $cm^{-2}$) | 3.9 V, 64 $\mu$Ah $cm^{-2}$ $\mu m^{-1}$ @32 $\mu Acm^{-2}$ (C/8) | this work |

**Characterization.** Cross-section SEM images were obtained with a FIB/SEM Helios 600i TFS system in a cryogenic stage (at about −150 °C). Grazing incidence X-ray diffractometry (GI-XRD) was performed on a Bruker D8 Discover diffractometer with Cu K$\alpha$ radiation at an incident angle of 3°. Electrochemical measurements were performed in an argon-filled glovebox (<1 ppm of $O_2$ and $H_2O$ levels, Inert Corp.) dedicated for electrochemical characterization. A Squidstat potentiostat (Admiral Instruments) was used to perform all electrochemical experiments. The cells were galvanostatically cycled between 4.25 and 3 V vs $Li^+$/Li at different C-rates.

## AUTHOR INFORMATION


### Corresponding Authors

**Jordi Sastre** − *Laboratory for Thin Films and Photovoltaics, Empa - Swiss Federal Laboratories for Materials Science and Technology, CH-8600 Dübendorf, Switzerland;* orcid.org/0000-0003-0866-0911; Email: jordi.sastrepellicer@empa.ch

**Yaroslav E. Romanyuk** − *Laboratory for Thin Films and Photovoltaics, Empa - Swiss Federal Laboratories for Materials Science and Technology, CH-8600 Dübendorf, Switzerland*; Email: yaroslav.romanyuk@empa.ch

### Authors

**Xubin Chen** − *Laboratory for Thin Films and Photovoltaics, Empa - Swiss Federal Laboratories for Materials Science and Technology, CH-8600 Dübendorf, Switzerland*

**Abdessalem Aribia** − *Laboratory for Thin Films and Photovoltaics, Empa - Swiss Federal Laboratories for Materials Science and Technology, CH-8600 Dübendorf, Switzerland*

**Evgeniia Gilshtein** − *Laboratory for Thin Films and Photovoltaics, Empa - Swiss Federal Laboratories for Materials Science and Technology, CH-8600 Dübendorf, Switzerland*

Complete contact information is available at: https://pubs.acs.org/10.1021/acsaem.1c01283

### Author Contributions

‡X.C. and J.S. contributed equally to this work.


### Notes

The authors declare no competing financial interest.

## ACKNOWLEDGMENTS

This work was supported by the joint Empa-Fraunhofer ISC project "IE4B" under the ICON funding line and the Swiss National Science Foundation (grant no. 200021_172764). We thank Dr. S.Gerstl for the cryo-FIB-SEM cross-section image and acknowledge support of the Scientific Center for Optical and Electron Microscopy (ScopeM) of the Swiss Federal Institute of Technology (ETHZ).

## REFERENCES


(1) Song, J.; West, W. *Handbook of Solid State Batteries*; World Scientific, 2015; Vol. 6; pp 593−625.

(2) Liao, Y.-T.; Yao, H.; Lingley, A.; Parviz, B.; Otis, B. P. A 3-$\mu$W CMOS Glucose Sensor for Wireless Contact-Lens Tear Glucose Monitoring. *IEEE J. Solid-State Circuits* **2012**, *47*, 335−344.

(3) Lee, H.; Kim, S.; Kim, K.-B.; Choi, J.-W. Scalable Fabrication of Flexible Thin-Film Batteries for Smart Lens Applications. *Nano Energy* **2018**, *53*, 225−231.

(4) Dudney, N. J. Solid-State Thin-Film Rechargeable Batteries. *Mater. Sci. Eng., B* **2005**, *116*, 245−249.

(5) Ribeiro, J. F.; Silva, M. F.; Carmo, J. P.; Gonçalves, L. M.; Silva, M. M.; Correia, J. H. In *Scanning Probe Microscopy in Nanoscience and Nanotechnology*; Bhushan, B., Ed.; Springer: Berlin, Heidelberg, 2012; Vol. 3, pp 575−619.

(6) He, X. *Flexible, Printed and Thin Film Batteries 2020−2030: Technologies, Markets and Players*; IDTechEx, 2020.

(7) Rumpel, M.; Machhaus, M.; Sastre, J.; Ziegler, S.; Chen, X.; Flegler, A.; Romanyuk, Y. E.; Giffin, G. A. How Interdiffusion Affects the Electrochemical Performance of LiMn2O4 Thin Films on Stainless Steel. *Mater. Adv.* **2021**, *2*, 2289.

(8) Julien, C. M.; Mauger, A.; Hussain, O. M. Sputtered $LiCoO_2$ Cathode Materials for All-Solid-State Thin-Film Lithium Micro-batteries. *Materials* **2019**, *12*, 2687.

(9) Filippin, A. N.; Lin, T.-Y.; Rawlence, M.; Zünd, T.; Kravchyk, K.; Sastre-Pellicer, J.; Haass, S. G.; Wäckerlin, A.; Kovalenko, M. V.; Buecheler, S. Ni−Al−Cr Superalloy as High Temperature Cathode Current Collector for Advanced Thin Film Li Batteries. *RSC Adv.* **2018**, *8*, 20304−20313.
(10) Glenneberg, J.; Andre, F.; Bardenhagen, I.; Langer, F.; Schwenzel, J.; Kun, R. A Concept for Direct Deposition of Thin Film Batteries on Flexible Polymer Substrate. *J. Power Sources* **2016**, *324*, 722−728.
(11) Glenneberg, J.; Kasiri, G.; Bardenhagen, I.; La Mantia, F.; Busse, M.; Kun, R. Investigations on Morphological and Electrochemical Changes of All-Solid-State Thin Film Battery Cells under Dynamic Mechanical Stress Conditions. *Nano Energy* **2019**, *57*, 549−557.
(12) Sepúlveda, A.; Speulmanns, J.; Vereecken, P. M. Bending Impact on the Performance of a Flexible Li4Ti5O12-Based All-Solid-State Thin-Film Battery. *Sci. Technol. Adv. Mater.* **2018**, *19*, 454−464.
(13) Song, S.-W.; Choi, H.; Park, H. Y.; Park, G. B.; Lee, K. C.; Lee, H.-J. High Rate-Induced Structural Changes in Thin-Film Lithium Batteries on Flexible Substrate. *J. Power Sources* **2010**, *195*, 8275−8279.
(14) Chen, X.; Sastre, J.; Rumpel, M.; Flegler, A.; Singhania, A.; Balta Bonner, J.; Hoffmann, P.; Romanyuk, Y. E. Photonic Methods for Rapid Crystallization of LiMn2O4 Cathodes for Solid-State Thin-Film Batteries. *J. Power Sources* **2021**, *495*, 229424.
(15) Yim, H.; Yu, S.-H.; Baek, S. H.; Sung, Y.-E.; Choi, J.-W. Directly Integrated All-Solid-State Flexible Lithium Batteries on Polymer Substrate. *J. Power Sources* **2020**, *455*, 227978.
(16) Rebohle, L.; Prucnal, S.; Reichel, D. *Flash Lamp Annealing: From Basics to Applications*; Springer Series in Materials Science; Springer International, 2019.
(17) Yoon, Y.; Park, C.; Kim, J.; Shin, D. Lattice Orientation Control of Lithium Cobalt Oxide Cathode Film for All-Solid-State Thin Film Batteries. *J. Power Sources* **2013**, *226*, 186−190.
(18) Nakazawa, H.; Sano, K.; Abe, T.; Baba, M.; Kumagai, N. Charge−Discharge Characteristics of All-Solid-State Thin-Filmed Lithium-Ion Batteries Using Amorphous Nb2O5 Negative Electrodes. *J. Power Sources* **2007**, *174*, 838−842.
(19) Ma, Y.; Chen, M.; Yan, Y.; Wei, Y.; Liu, W.; Zhang, X.; Li, J.; Fu, Z.; Li, J.; Zhang, X. Annealing of LiCoO2 Films on Flexible Stainless Steel for Thin Film Lithium Batteries. *J. Mater. Res.* **2020**, *35*, 31−41.
(20) Bedjaoui, M.; Martin, S.; Salot, R. Interconnection of Flexible Lithium Thin Film Batteries for Systems-in-Foil. In *2016 IEEE 66th Electronic Components and Technology Conference*; ECTC, 2016; pp 2082−2088.
(21) Lee, H.; Lim, K. Y.; Kim, K.-B.; Yu, J.-W.; Choi, W. K.; Choi, J.-W. Hybrid Thin-Film Encapsulation for All-Solid-State Thin-Film Batteries. *ACS Appl. Mater. Interfaces* **2020**, *12*, 11504−11510.
(22) Gotcu, P.; Seifert, H. J. Thermophysical Properties of LiCoO2−LiMn2O4 Blended Electrode Materials for Li-Ion Batteries. *Phys. Chem. Chem. Phys.* **2016**, *18*, 10550−10562.


https://doi.org/10.1021/acsaem.1c01283
*ACS Appl. Energy Mater.* 2021, 4, 5408−5414